

POWERFUL FLARES FROM RECOILING BLACK HOLES IN QUASARS

G. A. SHIELDS¹, E. W. BONNING^{1,2}

Submitted to ApJ August 1, 2007; revised February 25, 2008.

ABSTRACT

Mergers of spinning black holes can give recoil velocities from gravitational radiation up to several thousand km s⁻¹. A recoiling supermassive black hole in an AGN retains the inner part of its accretion disk. Marginally bound material rejoining the disk around the moving black hole releases a large amount of energy in shocks in a short time, leading to a flare in thermal soft X-rays with a luminosity approaching the Eddington limit. Reprocessing of the X-rays by the infalling material gives strong optical and ultraviolet emission lines with a distinctive spectrum. Despite the short lifetime of the flare ($\sim 10^4$ yr), as many as 10^2 flares may be in play at the present time in QSOs at redshifts ~ 1 to 3. These flares provide a means to identify high velocity recoils.

Subject headings: galaxies: active — quasars: general — black hole physics

1. INTRODUCTION

Simulations of binary black hole mergers show large recoil velocities (“kicks”) of the final merged black hole resulting from anisotropic emission of gravitational radiation [see, e.g., Campanelli et al. (2007b) for a summary and references]. The highest kick so far computed is 2500 km s⁻¹ for spin $a_* = 0.8$, with both black hole spins initially perpendicular to the orbital angular momentum and anti-aligned to each other (González et al. 2007; Tichy & Marronetti 2007). Campanelli et al. (2007b) predict a maximum recoil velocity of 4000 km s⁻¹ for equal mass black holes with maximal spin in this configuration. For a binary supermassive black hole ($\sim 10^8 M_\odot$) formed during a galactic merger (Begelman et al. 1980), the kick may displace the black hole from the galactic nucleus or eject it entirely (Merritt et al. 2004, and references therein). For a recoil occurring in an active galactic nucleus (AGN) with an accretion disk, the inner disk will remain bound to the black hole, providing fuel for continued AGN activity (Loeb 2007; Bonning et al. 2007). Such a ‘wandering QSO’ might be observed as a QSO displaced from the galactic nucleus or as a QSO with emission lines shifted relative to the galactic velocity. However, AGN rarely show displaced nuclei (Libeskind et al. 2006), and a search for Doppler-shifted broad line regions by Bonning et al. (2007) failed to detect any strong candidates for recoil. Bogdanović et al. (2007) argue that accretion by the merging black holes will align their spins in a way unfavorable for large kicks.

It is important to explore additional observational signatures of high velocity recoils that might help to confirm actual cases in nature. We note here that the sudden change in the black hole velocity leads to an increase in the energy of the disk matter that remains bound to the black hole, evaluated in the reference frame of the moving black hole. This can lead to a brief but powerful release of energy in soft X-rays and other forms of radiation (Shields, Bonning, & Salviander 2007). In §2, we discuss the mass and energy involved in the reforming

disk and the time scale and luminosity of the resulting “recoil flare.” In §3 we present a simple numerical simulation of the disk’s response to the kick. In §4 we discuss the observational appearance of the recoil flare, including soft X-ray emission from the primary shocks and secondary emission from photoionized gas and heated dust. In §5 we estimate the rate of occurrence of these events and the number of recoil flares that may be observable at the present time.

While this manuscript was undergoing revision, a paper appeared by Lippai et al. (2008) also predicting prompt shocks in an accretion disk around a recoiling black hole. Lippai et al. (2008) focus on smaller radii and shorter time scales, suitable for searching for optical counterparts of gravitational wave detections of merging supermassive black holes. Here we discuss the outermost bound disk with longer timescales with an eye to detecting recoil flares currently in play in the AGN population.

2. ENERGETICS

For a black hole merger taking place in an AGN, the accretion disk fueling the AGN will remain bound to the recoiling black hole inside the radius $R_b = (10^{18.12} \text{ cm}) M_8 v_{1000}^{-2}$ where the orbital velocity equals v_{kick} . Here, $M_8 = M_{\text{BH}}/10^8 M_\odot$ and $v_{1000} = v_{\text{kick}}/1000$ km s⁻¹. For an α disk (Shakura & Sunyaev 1973; Frank et al. 2002), the disk mass M_b that remains bound is

$$M_b = (10^{6.60} M_\odot) \alpha_{-1}^{-4/5} M_8^{1/4} \dot{M}_0^{7/10} R_{17}^{5/4} \quad (1)$$

or

$$M_b = (10^{8.02} M_\odot) \alpha_{-1}^{-4/5} M_8^{3/2} \dot{M}_0^{7/10} v_{1000}^{-5/2} \quad (2)$$

where \dot{M}_0 is the accretion rate in solar masses per year (Loeb 2007; Bonning et al. 2007). Here \dot{M} refers to the normal AGN phase *before* the tightening binary opens a gap in the disk at small radii $\sim 10^{2.4} r_g$, where $r_g \equiv GM_{\text{BH}}/c^2$ (Milosavljević & Phinney 2005; MacFadyen & Milosavljević 2008; Loeb 2007). The retained disk mass can fuel QSO activity over a disk consumption time t_d on the order of the viscous timescale of the outer bound disk where most of the mass resides. Once the inner gap has refilled, the post-merger

¹ Department of Astronomy, University of Texas, Austin, TX 78712; shields@astro.as.utexas.edu

² YCAA - Department of Physics, Yale University, New Haven, CT 06520; erin.bonning@yale.edu

accretion rate will resemble the pre-merger rate, giving $t_d \approx M_b/\dot{M}_0 \approx (10^8 \text{ yr}) \alpha_{-1}^{-4/5} M_8^{3/2} \dot{M}_0^{-3/10} v_{1000}^{-5/2}$.

Consider a recoil directed along the rotation axis (z-axis) of the accretion disk. Prior to the recoil, the material at radius R orbits with the Keplerian velocity v_{Kep} , specific angular momentum $l = R v_{\text{Kep}}$, and energy $E = -(1/2)v_{\text{Kep}}^2$. After the kick, the material still has the same angular momentum around the axis of symmetry; but it now has a velocity component $u_z = -v_{\text{kick}}$ along the negative z-axis in the reference frame moving with the black hole. (We use \mathbf{u} for velocities in the rest frame of the post-kick black hole.) This velocity adds in quadrature to the orbital velocity $u_\phi = v_{\text{Kep}}$. The total energy per unit mass is now $E' = E + (1/2)v_{\text{kick}}^2$. This applies at each radius that remains bound to the hole, and therefore the total energy of the disk material has increased by an amount $E_{\text{kick}} = E' - E = (1/2)M_b v_{\text{kick}}^2$. Because the angular momentum is unchanged, the bound material will eventually settle into circular orbits at the original radius and binding energy. The excess energy that the material has immediately after the kick must therefore be dissipated. We argue below that this dissipation will in large part involve shocks at $\sim v_{\text{kick}}$, leading to an outburst or “recoil flare” with $E_{\text{flare}} = \xi_E E_{\text{kick}}$, where ξ_E is of order unity. The energy associated with a disk with the mass given by Equation 2 is

$$E_{\text{flare}} = (10^{57.0} \text{ erg}) \alpha_{-1}^{-4/5} M_8^{3/2} \dot{M}_0^{7/10} v_{1000}^{-1/2} \xi_E. \quad (3)$$

A more rigorous calculation takes account of the slowing of the black hole as it shares linear momentum with the bound disk mass. When the disk has returned to its equilibrium state, the disk and black hole share a velocity $v_z = v_{\text{kick}}(1 + M_b/M_{\text{BH}})^{-1}$; and the energy dissipated is $E_{\text{kick}} = (1/2)M_b v_{\text{kick}}^2 (1 + M_b/M_{\text{BH}})^{-1}$. The kinetic energy lost by the black hole provides the energy radiated and the kinetic energy associated with the motion of the disk in the z-direction. For $M_b/M_{\text{BH}} < 1$ as considered here, most of the energy goes to radiation. Additional energy will be imparted to disk material outside R_b that is drawn toward the moving black hole but remains unbound. We ignore these complications here.

Following a perfectly axial kick, the particles at any radius will follow non-intersecting elliptical orbits in the reference frame of the moving black hole, and a number of orbits may pass before the excess energy is dissipated. For a kick inclined to the disk axis, the available energy will be similar (see §3); but particles initially at radii with v_{Kep} not greatly larger than v_{kick} (i.e., R or order R_b) will have a post-kick velocity in the black hole’s frame that is a strong function of azimuth in the disk. These particles will follow orbits with a range of inclinations and eccentricities, and the disk will be not merely perturbed but seriously disrupted. On approximately the orbital period, material from different parts of the disk will collide and shock at velocities of order v_{kick} . Marginally bound material will lag substantially behind the recoiling hole and then fall back into the disk with velocity $\sim v_{\text{kick}}$. More tightly bound material in the inner disk will have its orbits perturbed more modestly and may shock more gently if at all (Loeb 2007; Lippai et al. 2008). However, for the mass surface density underlying Equation 1, a majority of the bound mass lies outside $R = 0.5R_b$, and we expect that much of the excess en-

ergy represented by E_{flare} will be dissipated in shocks at velocities of order v_{kick} (see §3). The temperature of an AGN disk at relevant radii is $< 10^4$ K, with a sound speed $c_s < 10 \text{ km s}^{-1}$. Thus, collisions at even a fraction of v_{kick} are highly supersonic.

We take the time scale for the recoil flare to be

$$t_{\text{flare}} = P_b \xi_t = (10^{3.4} \text{ yr}) M_8 v_{1000}^{-3} \xi_t, \quad (4)$$

where $P_b = 2\pi R_b/v_{\text{kick}}$ is the Keplerian orbital period at R_b . The factors ξ_E and ξ_t express the uncertainty in the radiated energy and time scale. Below we estimate $\xi_E \approx 1$ and $\xi_t \approx 2$ on the basis of simple numerical simulations. In §4 we argue that the flare may be observable for ξ_E as small as 10^{-2} .

The power associated with this dissipation is about $E_{\text{flare}}/t_{\text{flare}}$ or

$$L_{\text{flare}} = (10^{46.1} \text{ erg s}^{-1}) \alpha_{-1}^{-4/5} M_8^{1/2} \dot{M}_0^{7/10} v_{1000}^{5/2} (\xi_E/\xi_t). \quad (5)$$

For comparison, the bolometric luminosity of the AGN is

$$L_{\text{bol}} = \epsilon \dot{M} c^2 f_g = (10^{45.8} \text{ erg s}^{-1}) \dot{M}_0 f_g \quad (6)$$

for efficiency $\epsilon = 0.1$. The factor $f_g \approx 10^{-1}$ allows for suppression of the central accretion rate by the inner gap formed by the binary (MacFadyen & Milosavljević 2008). The ratio is

$$L_{\text{flare}}/L_{\text{agn}} = 10^{0.3} \xi_t^{-1} f_g^{-1} \alpha_{-1}^{-4/5} M_8^{1/2} \dot{M}_0^{-3/10} v_{1000}^{5/2}. \quad (7)$$

Here and below we take $\xi_E = 1$. The power of the flare can substantially exceed that of the AGN. This is true because a large part of the disk mass shocks on roughly the orbital period, giving a mass shocked per unit time much larger than the central accretion rate, which is driven by the comparatively long viscous timescale. This disparity in time scale offsets the lower energy per unit mass in the shocks, compared with the black hole accretion efficiency of $\sim 0.1c^2$.

The post-shock temperature will be

$$T_{\text{shock}} = (10^{6.9} \text{ K}) (v_{1000})^2 = (0.7 \text{ keV}) v_{1000}^2 \quad (8)$$

(Osterbrock & Ferland 2006). The flare lifetime is shorter for higher recoil velocities, but the luminosity is higher and the X-rays harder.

The disk mass estimated in Equation 2 is subject to a number of uncertainties. We have extrapolated the standard α -disk surface density Σ to radii where the disk is too cool for the assumed opacity to apply. However, Σ is a weak function of opacity (Goodman & Tan 2004). For larger M_{BH} and lower v_{kick} , the stability limit $M_b < M_{\text{BH}}$ becomes important (Loeb 2007). If we let R_{lim} and v_{lim} refer to the radius and orbital velocity within which the α -disk mass equals M_{BH} , then from Equation 1 we have

$$R_{\text{lim}} = (10^{18.11} \text{ cm}) \alpha_{-1}^{16/25} M_8^{3/5} \dot{M}_0^{-14/25} \quad (9)$$

and

$$v_{\text{lim}} = (10^{3.01} \text{ km s}^{-1}) \alpha_{-1}^{-8/25} M_8^{1/5} \dot{M}_0^{7/25}. \quad (10)$$

This limits the energy and luminosity of the flare, but it remains a powerful event.

A further complication is the role of the disk’s self-gravity at larger radii (Goodman 2003). For an α -disk,

this comes into play where the Toomre stability parameter reaches unity, $r_Q \approx 10^{3.6} r_g$ and a Keplerian velocity $v_Q \approx 10^{3.7} \text{ km s}^{-1}$. The consequences for the disk structure outside r_Q are unclear. If the surface density of the disk is severely reduced at radii $\sim 10^5 r_g$ of interest here, then the amount of shocked gas and the power in the flare will be correspondingly reduced; but clumping of the disk gas should not greatly affect our conclusions. If the disk regulates itself at $Q \approx 1$, then Goodman finds a radial dependence of $\Sigma \propto r^{-1}$ or $r^{-3/2}$ rather than the $r^{-3/4}$ dependence underlying Equation 1. Such a modification of the disk mass near R_b would affect our quantitative results but leave the recoil flare a readily observable phenomenon. Goodman summarizes a variety of observational indications that gas disks in AGN do in fact extend to parsec scales. We proceed on the assumption that a gas disk exists at these radii, but we caution that the mass is uncertain.

3. NUMERICAL SIMULATION

In order to test our assumption of high velocity shocks, we have carried out a simple numerical simulation of the response of the disk to the black hole recoil. We simulated the initial disk as a collection of collisionless particles in Keplerian orbit in the $x - y$ plane, and followed the motion of the particles and black hole in 3 dimensions with the aid of an N-body code by (Aarseth 1985), adapted to our purposes. We worked in dimensionless units with $G = 1$, a particle mass $m_p = 1$, and $M_{\text{BH}} = 10^5$. The initial disk had zero thickness. (An AGN disk at the radii of interest has $H/R \ll 1$; and for the non-axial kicks of interest, post-kick motions out of the original plane far exceed the initial disk thickness and internal sound speed.) We ignored the gravitation force of the disk on itself and on the black hole. We modeled the case of a kick in the $y - z$ plane at 45 degrees to the rotation axis. In the units of our model, the radial limits of the disk were $R_1 = 10$ and $R_2 = 50$. We took $v_{\text{kick}} = 65$, giving $R_b = 23.6$, intermediate between R_1 and R_2 . Test calculations reproduced a stable disk around a stationary hole, and the nonintersecting nature of orbits for an axial kick. Note that the choice of particle mass and radius scale are arbitrary. The simulation is defined by the direction of the kick and the ratios R_1/R_b and R_2/R_b . Scaling to specific astrophysical parameters is straightforward using the expressions in §2.

In order to test for collisions, we associated a fixed radius r_p of unity with each particle. The initial disk comprised concentric rings of particles, separated by $2r_p$ in radius and in azimuth. Thus, the disk particles are initially just touching their neighbors. This arrangement gave us about 2000 particles. We defined a ‘collision’ to occur when two particles passed within r_p of each other.

The expected behavior can be visualized in the rest frame of the black hole just after the kick. The particles have velocity components $-v_{\text{kick},y}$ and $-v_{\text{kick},z}$ added to their original orbital velocity. The total y -component in this frame is $u_y = -v_{\text{Kep}} \sin(\phi) - v_{\text{kick},y}$, which varies strongly with azimuth ϕ . The binding energy per unit mass in the frame of the hole is now $E = -GM_{\text{BH}}/R + (1/2)u^2$, where u is the particle’s velocity in the rest frame of the hole. This determines the orbital semi-major axis, $a = 2GM/(-E)$, and period

$P = 2\pi a^{3/2}(GM)^{-1/2}$. For all radii in our simulation, the material in a given ring is bound to the hole for a range of ϕ and unbound at other azimuths.

In the units of our model, the orbital period at R_b is $P_b = 2.28$, and this sets the time scale of the recoil flare. We ran our simulation from $t = 0$ to $t = 14$. Figures 1 - 3 show the positions of the particles at several times during the evolution. The more tightly bound material at smaller radii follows the hole relatively closely. More weakly bound material lags before ultimately returning to periastron, where it is likely to collide with other portions of the disk material. The bound particles experience collisions at high velocity with other particles originating at substantially different locations in the original disk. We take the energy dissipated per collision to be $(1/2)v_{\text{rel}}^2 m_p$.

Figure 4 shows the power per unit time produced by the colliding particles, computed by summing the energy for 100 consecutive collisions and dividing by the elapsed time. The power level rises over a time $\sim P_b$, and persists for several times P_b . The power at later times is exaggerated because of repeat collisions involving particles that have completed multiple orbits. The r.m.s. relative velocity of the colliding particles, weighted by the collision energy, rises from $v/v_{\text{kick}} = 0.3$ near the start of the run to 0.9 at $t = P_b$ and 1.4 for the entire run. This characterizes which shock velocities dominate the power and the shock temperature and spectrum.

Two theoretical light curves are shown for comparison in Figure 4. (1) Here each bound particle was assumed to shock exactly one orbital period after the kick, releasing an energy $(1/2)m_p v_{\text{kick}}^2$. The events were ordered in terms of P and binned in groups of 50 particles to calculate the luminosity. (2) The smooth curve in Figure 4 represents an analytic solution for an axial kick. The post-kick orbital period increases monotonically and approaches infinity as R approaches R_b . We assume that the mass originating at each radius shocks at velocity v_{kick} at time $t = P$, giving a power $L = (1/2)v_{\text{kick}}^2 dM/dt$, where $dM/dt = dM/dP = 2\pi \Sigma R dR/dP$, and $P(R)$ is given by the post-kick binding energy in the frame of the moving black hole. For constant surface mass density Σ , this gives

$$\dot{M} = (4/3)(M_b/P_b)\zeta^{-5/3}/(\zeta^{-2/3} + 1)^3, \quad (11)$$

where $\zeta \equiv t/P_b$. This decreases as $\dot{M} \propto t^{-5/3}$ at late times, a qualitatively similar decline to comparison curve (1) above. This case is given for reference only, as an axial kick will dissipate slowly (see above); and for smaller radii (having $P \ll P_b$) the orbits are less radically perturbed. Despite the approximations, the various light curves agree at the factor-of-two level as to the power expected at times of one to several times P_b .

Integrated over the run, the power dissipated in collisions is $E_{\text{coll}} = 2.8 \times 10^6$, somewhat exaggerated by repeat collisions at later times. We may compare this with the overall energetics of the disk. Of the 1968 particles in the model disk, 831 remain bound to the hole, so the bound mass is $M_{b0} = 831$. This compares with 381 particles that are initially inside R_b ; for the tilted kick, a substantial part of the mass outside R_b remains bound to the black hole. The binding energy of the bound mass immediately after the kick is $E_{b0} = -1.28 \times 10^6$, and its total angular momentum is $L_{b0} = 1.07 \times 10^6$. Let us as-

sume conservation of angular momentum for the bound mass in the aggregate as it settles into a circular disk around the recoiling hole. The shallowest binding energy for this mass and angular momentum occurs for a narrow orbiting ring, giving a radius $R_{\text{ring}} = 16.6$ and energy $E_{\text{ring}} = -2.51 \times 10^6$. In this case, the energy that must be dissipated to reach this configuration is $\Delta E = E_{\text{b0}} - E_{\text{ring}} = 1.23 \times 10^6$. Alternatively, if the final state is a uniform disk with a sharp outer boundary, then $E_{\text{final}} = (32/25)E_{\text{ring}} = -3.21 \times 10^6$ and the dissipated energy is $\Delta E = 1.93 \times 10^6$. These values are comparable to the simple estimate $\Delta E = (1/2)M_{\text{b0}}v_{\text{kick}}^2 = 1.76 \times 10^6$, using here the actual bound mass for the tilted kick. This supports a value $\xi_E \approx 1$ in Equation 3.

For our model, the most tightly bound quarter of the particles have a post-kick orbital period $P < 1.1P_b$, one half of all the bound particles have period $P < 2.4P_b$, and the most weakly bound quarter of the particles have $P > 5.4P_b$. This suggests that, to characterize the main surge of the flare, we may take $\xi_t \approx 2$ in Equation 4. There is some material with arbitrarily weak binding energy after the kick. This material lags far behind the moving hole, giving a prolonged tail to the impact rate. In our numerical model, the bulk of the shock power corresponds to collisions occurring at radii near or inside R_b ; the mean collision radius, weighted by collision energy, is ~ 12 or $0.5R_b$, with little variation during the run. The collisions typically involve pairs of bound particles that originate at substantially different radii near or outside R_b , and substantially different azimuths. These particles move on quite eccentric orbits, and the collisions producing most of the power typically occur not far from periastron.

We conclude that a non-axial kick will severely disrupt the orbits of the mass elements in the disk at radii $\sim R_b$, leading to strong shocks. A physically realistic hydrodynamical simulation will be needed to compute a more detailed light curve. However, our simulation supports the approximate energetics outlined in §2.

4. APPEARANCE

Equation 8 suggests that shocked gas in the post-kick disk will release its energy largely in the form of thermal soft X-rays, with $kT \approx 0.7$ keV for $v_{\text{kick}} = 1000$ km s⁻¹, or 0.2 keV for $v_{\text{kick}} = 500$ km s⁻¹. Subject to the redshift and absorption by the surrounding material, this radiation could be observable.

Consider a QSO with $M_{\text{BH}} = 10^8 M_\odot$ accreting at $10^{-0.5} M_\odot \text{ yr}^{-1}$ (giving $L/L_{\text{Ed}} \approx 10^{-0.8}$) before the inner gap forms. Then $v_{\text{lim}} = 750$ km s⁻¹, and for a kick velocity of 1000 km s⁻¹ the bound disk mass of $10^{7.7} M_\odot$ is less than M_{BH} . The radius of the retained disk in this case is $R_b = 10^{18.1}$ cm, and the surface density is $\Sigma \approx M_b/\pi R_b^2 = 10^{4.2}$ g cm⁻². The above discussion suggests that, for times $t > P_b$, the recoil flare has the character of material on highly eccentric orbits impacting the disk at radii $\sim R_b$. For the parameters just assumed, $t_{\text{flare}} \approx \xi_t P_b = (10^{3.4} \text{ yr})\xi_t$ or ~ 5000 yr for $\xi_t = 2$. The corresponding mass infall rate is $\dot{M}_{\text{flare}} \approx M_b/t_{\text{flare}} = (10^{4.0} M_\odot \text{ yr}^{-1})$. This large rate of mass undergoing shocks is, of course, the basis of the large power of the flare. The density of the infalling material is subject to uncertain geometrical details, but a

simple estimate is $\rho \approx \dot{M}_{\text{flare}}/(2\pi R_b^2 v) = 10^{-15.2}$ g cm⁻³, or $N = \rho/m_H = (10^{8.6} \text{ cm}^{-3})$. The cooling time will be $\sim 10^{-2}$ yr, so that the material will cool in a relatively narrow zone on the scale of R_b . The local energy flux in the X-ray flare is $F_{\text{flare}} \approx (1/2)\rho v^3 \approx 10^{8.5}$ erg cm⁻² s⁻¹. The column density in the impacting stream is $\sim \rho R_b \approx 10^{2.9}$ g cm⁻². The optical depth due to photoelectric absorption by H, He, and heavy elements will be large, and the X-rays may be unable to penetrate the enveloping inflow. However, the luminosity of the shocked flow, $L_{\text{flare}} \approx (10^{45.4} \text{ erg s}^{-1})$, is close to the Eddington limit. This raises the possibility of radiation driven outflows, although the energy available is insufficient to expel the entire disk mass. Given these outflows and the complex geometry of the infalling material, there may be clear lines of sight on which the X-rays escape. While the shock temperature is high, the effective temperature corresponding to F_{flare} is only $T_{\text{eff}} = (F_{\text{flare}}/\sigma)^{1/4} \approx 10^{3.2}$ K. This underscores the sensitivity of the observed appearance of the flare to the nature of the reprocessing that occurs in the surrounding material.

For an estimate of the spectrum of the cooling shocked gas, we computed a coronal equilibrium model using version 07.02.00 of the photoionization code CLOUDY, most recently described by Ferland et al. (1998). We used $T = 10^7$ K, $N = 10^{9.6} \text{ cm}^{-3}$, and solar abundances. (This corresponds to a pre-shock velocity 1100 km s⁻¹ and density of 10^9 cm^{-3} .) Much of the total cooling is thermal bremsstrahlung. There are many strong emission lines, including lines of Fe XVII to Fe XX at 12 to 15 Å, each with several percent of the total energy (see Figure 5). If not totally absorbed by the infalling gas, this should be recognizable as a unique spectrum for a point source in a galactic nucleus. Comptonization should be insignificant, and the flare will not emit hard X-rays. There could, however, be hard X-rays if the AGN luminosity is not entirely shut off by the inner gap in the disk at the time of the merger.

The X-ray luminosity will photoionize the infalling material approaching the shock. The local energy flux in the X-ray flare directed into the infalling gas is $F_{\text{flare}} \approx 10^{8.8}$ erg cm⁻² s⁻¹, giving an ionizing photon flux of $\phi_i \approx 10^{18.2}$ cm⁻² and an ionization parameter $U = \phi_i/Nc = 0.05$. We have computed photoionization models with CLOUDY for this precursor zone. We used the coronal model emission as the ionizing spectrum with flux $10^{8.8}$ erg cm⁻² s⁻¹, a gas density $N = 10^9 \text{ cm}^{-3}$, and a cutoff column density $10^{23.5} \text{ cm}^{-2}$. The photoionized depth in this pre-shock flow is $\sim 10^{13.7}$ cm, again narrow compared to R_b . The high ionization parameter and hard ionizing spectrum give strong ultraviolet emission lines of highly ionized species (see Table 1 and Figures 6 and 7). The Ly α line carries 11% of the incident energy flux, and O VI and C IV are comparably strong. The H β and C IV lines respectively have equivalent widths of ~ 780 and 6100 Å in terms of the diffuse continuum of the precursor alone. The Balmer and helium lines are affected by large optical depths. Based on the coronal equilibrium model, the shock will contribute an additional 12% to the continuum at H β and 30% at $\lambda 1550$, slightly reducing the equivalent widths. The high density suppresses forbidden line emission. Aside from

this and transfer effects in some lines, the spectrum is not strongly sensitive to density, because the shock velocity alone determines the post shock temperature and also the ionization parameter of the precursor.

We also computed CLOUDY models for a case corresponding to $v_{\text{kick}} = 500 \text{ km s}^{-1}$. We took $M_8 = 10^{-0.5}$ and $\dot{M}_0 = 10^{-0.7}$ to conform to the self-gravity limit. This gives $t_{\text{flare}} = 10^{4.1} \text{ yr}$ for $\xi_t = 2$, and a preshock gas density of $N = 10^{8.1} \text{ cm}^{-3}$ estimated as above. Table 1 shows the emission-line intensities of the precursor ionized by the emission from a $10^{6.3} \text{ K}$ coronal model for the shocked gas. Many of the same strong emission lines occur, such as $\text{H}\beta$, $\text{Ly}\alpha$, and C IV . However, O VI is much weaker, due to a lower level of ionization and a lower electron temperature. Thus, the high ionization line intensities offer a potential diagnostic of the shock velocity and hence v_{kick} . Forbidden lines such as $[\text{O III}] \lambda 5007$, $[\text{O III}] \lambda 4363$, and $[\text{Ne V}] \lambda 3426$ have intensities of 0.5 to 1.0 times $I(\text{H}\beta)$ because of the lower density.

We may estimate the relative luminosity of the recoil flare at specific wavelengths with the aid of Equation 7. In the optical, a typical AGN energy distribution gives $\lambda L_\lambda(5100) = 0.11 L_{\text{bol}}$ (Kaspi et al. 2000). The photoionized precursor by itself has $\lambda L_\lambda(5100) = 0.03 L_{\text{bol}}^{\text{flare}}$ based on the CLOUDY model. Using these factors in equation 7, we have

$$\lambda L_\lambda^{\text{flare}} / \lambda L_\lambda^{\text{AGN}} = C_\lambda \xi_t^{-1} f_g^{-1} \alpha_{-1}^{-4/5} M_8^{1/2} \dot{M}_0^{-3/10} v_{1000}^{5/2}, \quad (12)$$

with $C_\lambda = 10^{-0.3}$ for $\lambda 5100$. A similar calculation for $\lambda 1550$ gives $C_\lambda = 10^{-0.6}$. Therefore, the flare continuum is comparable with the AGN continuum if $f_g = 1$ or dominant if f_g is small. This in turn implies that the equivalent widths of the flare emission lines remain large relative to the total observed continuum, including the AGN component. In the composite QSO spectrum of (Vanden Berk et al. 2001), the equivalent widths of $\text{H}\beta$, C IV , $\text{Ly}\alpha$, and O VI are 46, 24, 93, and 10 \AA , respectively, mostly in the broad line component. With their large equivalent widths and narrow profiles, the flare emission lines should be prominent in the total spectrum. Indeed, they remain conspicuous even if the flare contribution is two orders-of-magnitude weaker than estimated here, relative to the AGN. The number of detectable flares in play could be increased by as much as an order of magnitude by the prolonged arrival of weakly bound material catching up to the black hole (see §3). The line widths will be $\sim v_{\text{kick}}$, typically 500 to 1000 km s^{-1} for flares likely to be observed (see below). These line widths resemble those of Narrow Line Seyfert 1 (NLS1) objects or the lines from the traditional narrow line region (NLR) of AGN. However, the lines of the recoil flare will be distinctive, showing (1) potentially large equivalent widths, (2) weakness or absence of forbidden lines such as $[\text{O III}] \lambda 5007$, (3) strong $\text{He II} \lambda 4686$ and possibly $\text{O VI} \lambda 1035$, and (4) likely velocity shifts and asymmetries of order v_{kick} . Absorption by dust in the surrounding disk material may be important. The disk temperature near R_b is low enough before the kick for dust to exist, and the energy flux from the shocks may not be enough to evaporate refractory grains.

We may similarly estimate the prominence of the soft X-rays from the primary shocked gas. For the AGN continuum at 0.3 keV , Laor et al. (1997) find an av-

erage $\nu L_{\nu,0.3} = 10^{-1.0} \nu L_\nu(3000 \text{ \AA})$; and by the above conversions, this gives $\nu L_{\nu,0.3} = 10^{-1.8} L_{\text{bol}}^{\text{AGN}}$. From the CLOUDY model for $T = 10^7 \text{ K}$, we find $R_{0.3} \equiv \nu L_{\nu,0.3}^{\text{flare}} / L_{\text{bol}}^{\text{flare}} = 10^{-1.0}$. Combining these expressions with Equation 7, we find

$$\nu L_{\nu,0.3}^{\text{flare}} / \nu L_{\nu,0.3}^{\text{AGN}} = 10^{1.1} (R_{0.3}/10^{-1}) \xi_t^{-1} f_g^{-1} \alpha_{-1}^{-4/5} M_8^{1/2} \dot{M}_0^{-3/10} v_{1000}^{5/2}. \quad (13)$$

If a substantial fraction of the X-ray radiation from the shocks is able to reach the observer, the object will stand out as an exceptionally strong source in soft X-rays, relative to its optical and ultraviolet luminosity. This remains true for $v_{\text{kick}} = 500 \text{ km s}^{-1}$, giving $T_{\text{shock}} = 10^{6.3} \text{ K}$. Our coronal equilibrium model at this temperature shows a continuum dropping at $\lambda < 30 \text{ \AA}$ and many emission lines forming a pseudocontinuum at 30 to 60 \AA . In the vicinity of 40 \AA (0.3 keV), the power in the lines corresponds to $R_{0.3} = 10^{-0.5}$, again giving a large ratio of soft X-rays to optical continuum.

The unified model of AGN posits a thick dusty torus that surrounds the emitting core at a radius of one or several parsecs (Antonucci & Miller 1985). This torus will intercept and reprocess a substantial fraction of the X-ray and optical-ultraviolet radiation from the reforming accretion disk. A large part of the flare luminosity should therefore appear as infrared radiation from dust.

5. RATE OF OCCURRENCE

The number of recoil flares currently observable depends on the rate of mergers, the probability of kicks of various velocities, and the flare duration at a given velocity. Let dN/dt be the merger rate per year of observer time in some range of M_{BH} and redshift z ; and let f_v be the fraction of mergers giving a kick velocity greater than v . The number of kicks currently observable is roughly $N_{\text{flare}} \approx (dN/dt) [t_{\text{flare}}(1+z)] f_v$, where the factor $1+z$ allows for the observed duration of a flare with intrinsic duration t_{flare} . For mergers of two black holes with equal spin parameter $a_* \equiv J/M = 0.9$ and roughly equal masses satisfying $q \equiv m_2/m_1 \gtrsim 0.2$, Schnittman & Buonanno (2007) find $f_{500} = 0.31$ and $f_{1000} = 0.08$. These results rely on uncertain assumptions about the merger details but provide an approximate basis for estimating the number of high velocity recoils.

Two alternative estimates of N_{flare} are as follows:

(1) Sesana et al. (2004, 2007) and Volonteri (2007) compute binary merger rates in hierarchical merger simulations normalized to the observed QSO luminosity function. Volonteri (2007, personal communication) has kindly provided merger rates for mass ratios $q > 0.2$ for the various seed black hole scenarios of Sesana et al. (2007). In the ‘‘VHM’’ scenario (small seeds), the event rate per observer year for $1 < z < 3$ is $\sim 0.08 \text{ yr}^{-1}$ for $(m_1 + m_2)$ in the range 10^7 to $10^8 M_\odot$ and 0.014 yr^{-1} in the range 10^8 to $10^9 M_\odot$. The event rate is about 3 times smaller in the other scenarios. The rates drop rapidly for $z < 1$. Let f_{QSO} be the fraction of these mergers that are sufficiently gas-rich to fuel QSO activity. For the 10^7 to $10^8 M_\odot$ range, we have $t_{\text{flare}} \approx 800 \xi_t \text{ yr}$ at $v_{\text{kick}} = 1000 \text{ km s}^{-1}$ for $M_{\text{BH}} = 10^{7.5} M_\odot$. Then in the VHM scenario we expect to see roughly $15 \xi_t f_{\text{QSO}}$ events currently in play. For $v_{\text{kick}} > 500 \text{ km s}^{-1}$, we

expect $\sim 500\xi_t f_{\text{QSO}}$ events in play, taking account of the longer flare duration and the larger fraction of recoils above the lower kick velocity. For 10^8 to $10^9 M_\odot$, the limit $M_b < M_{\text{BH}}$ comes into play for a typical value $L/L_{\text{Ed}} = 10^{-0.5}$ (e.g., Salviander et al. 2007), and this affects t_{flare} . If we take $t_{\text{flare}} \approx 2\pi R_{\text{lim}}/v_{\text{lim}}$ (equations 9 and 10), then we expect $\sim 8 f_{\text{QSO}}$ flares in play above 1000 km s^{-1} and $\sim 33 f_{\text{QSO}}$ above 500 km s^{-1} . These numbers could be several times larger if the disk extends beyond R_{lim} with a mass remaining below M_{BH} .

(2) Haehnelt (1994) derived the black hole merger rate from the QSO luminosity function assuming $L = L_{\text{Ed}}$, one event per black hole, and a QSO lifetime of $t_{\text{QSO}} = 10^{7.6} \text{ yr}$ (the ‘‘Salpeter time’’ for black hole growth). At M_{BH} between 10^7 and $10^8 M_\odot$, Haehnelt finds 0.016 events per year of observer time for $z < 3$, giving roughly $3\xi_t$ flares in play for $v_{\text{kick}} > 1000 \text{ km s}^{-1}$, and $94\xi_t$ in play above 500 km s^{-1} . Uncertainties in this estimate of N_{flare} include the assumed value of L/L_{Ed} and the QSO lifetime, the flare duration, and the number of obscured QSOs. However, we do not need the factor f_{QSO} because the calculation is based on observed QSOs.

Despite the uncertainties, it appears likely that several flares above $10^7 M_\odot$ are currently observable. We emphasize that this rests on the assumption that the black hole merger occurs while the QSO accretion disk is in place.

For a $10^8 M_\odot$ hole in a QSO shining at $0.3L_{\text{Ed}}$ at $z = 2$ (prior to formation of the inner gap), the received flux from the flare is $\sim 10^{-12.8} \text{ erg cm}^{-2} \text{ s}^{-1}$ for $\xi_t = 2$. The observed spectrum will be softened by the redshift, but a considerable fraction of the radiation should still be received at photon energies above 0.2 keV. At $10^{-12.8} \text{ erg cm}^{-2} \text{ s}^{-1}$, Hasinger et al. (2005) find ~ 2 soft X-ray sources (0.5 to 2 keV) per square degree, so that the recoil flares would need to be identified from among roughly 10^5 other sources of similar flux. The unique spectrum of the flare should aid recognition.

An optical search for recoil flares could target the strong, narrow emission lines in the rest optical and ultraviolet. For $t_{\text{QSO}} = 10^{7.6} \text{ yr}$, the fraction of QSOs in the recoil flare stage from Equation 4 is

$$N_{\text{flare}}/N_{\text{QSO}} = 10^{-3.2} M_8 v_{1000}^{-3} \xi_t f_v. \quad (14)$$

This gives $N_{\text{flare}}/N_{\text{QSO}} = 10^{-4.3} M_8 \xi_t$ for $v_{1000} = 1$ and $10^{-3.7} M_8 \xi_t$ for $v_{1000} = 0.5$. Thus, recoil flares may be observable in about one in 10,000 QSOs, and one or more examples may be present in existing large spec-

troscopic surveys. For example, the SDSS DR5 QSO Catalog (Schneider et al. 2007) contains 77,429 objects with a median redshift $z = 1.48$ over $\sim 5740 \text{ deg}^2$ of sky. About 10^4 of these objects have $z < 0.8$ so that $\text{H}\beta$ is accessible, and many have $z > 1.7$ so that C IV is accessible. The higher redshift objects typically have relatively high luminosity and black hole masses $\sim 10^{8.5} M_\odot$ or higher, so that the self-gravity limit on the accretion disk is significant. However, the discussion in §4 suggests that, even if the disk mass around R_b is much less than assumed in Equation 5, the flare emission lines still could be prominent. The observed QSO population serves as the parent population for the recoil flares, but the AGN luminosity may be dimmed several magnitudes by the inner gap at the time of the recoil. This will complicate the detection of AGN undergoing recoil flares and their inclusion in QSO surveys.

6. CONCLUSION

Merged black holes with high recoil velocities can carry a large mass of gas in an accretion disk that remains bound to the black hole. The kick velocity gives the disk material a boost in energy, relative to the moving hole, that will in substantial part be dissipated in shocks within a few orbital periods as the more weakly bound material rejoins the moving disk. This results in a soft X-ray flare lasting thousands of years with a luminosity rivaling or exceeding the AGN luminosity. The X-rays will be heavily absorbed, at least along some lines of sight, and the energy re-emitted in line and continuum emission from photoionized gas and infrared radiation from heated dust. A number of recoil flares may be currently observable. Observational detection of such an event would provide an important confirmation of the occurrence in nature of high velocity recoils. Detailed simulations of the observational appearance of these recoil flares are needed to aid in identifying such objects in surveys at X-ray and other wavelengths.

We thank Marta Volonteri for providing numerical results and Ski Antonucci, Omer Blaes, Richard Matzner, Milos Milosavljević, and Meg Urry for helpful discussions. EWB acknowledges partial support by Marie Curie Incoming European Fellowship contract MIF1-CT-2005-008762 within the 6th European Community Framework Programme.

REFERENCES

- Aarseth, S. J. 1985, in *Multiple Timescales*, ed J U Brackbill & B. I. Cohen, Orlando: Academic Press, p 377
- Antonucci, R. R. J., & Miller, J. S. 1985, *ApJ*, 297, 621
- Baker, J. G., Boggs, W. D., Centrella, J., Kelly, B. J., McWilliams, S. T., Miller, M. C., & van Meter, J. R. 2007, *ApJ*, 668, 2
- Baker, J. G., Centrella, J., Choi, D.-I., Koppitz, M., van Meter, J. R., & Miller, M. C. 2006, *ApJ*, 653, L93
- Begelman, M. C., Blandford, R. D., & Rees, M. J. 1980, *Nature*, 287, 307
- Bogdanović, T., Reynolds, C. S., & Miller, M. C. 2007, *ApJ*, 661, L147
- Bonning, E. W., Shields, G. A., & Salviander, S. 2007, *ApJ*, 666, L13
- Campanelli, M., Lousto, C., Zlochower, Y., & Merritt, D. 2007, *Phys. Rev. Lett.*, 98, 231102
- Ferland, G. J., Korista, K.T., Verner, D.A., Ferguson, J.W., Kingdon, J.B. & Verner, E.M. 1998, *PASP*, 110, 761
- Frank, J., King, A., & Raine, D. J. 2002, *Accretion Power in Astrophysics: Third Edition* (Accretion Power in Astrophysics, by Juhan Frank and Andrew King and Derek Raine, pp. 398. ISBN 0521620538. Cambridge, UK: Cambridge University Press, February 2002.)
- González, J. A., Hannam, M., Sperhake, U., Brügmann, B., & Husa, S. 2007, *Physical Review Letters*, 98, 231101
- Goodman, J. 2003, *MNRAS*, 339, 937
- Goodman, J., & Tan, J. C. 2004, *ApJ*, 608, 108
- Haehnelt, M. G. 1994, *MNRAS*, 269, 199
- Hasinger, G., Miyaji, T., & Schmidt, M. 2005, *A&A*, 441, 417
- Kaspi, S. et al. 2000, *ApJ*, 533, 631
- Libeskind, N. I., Cole, S., Frenk, C. S., & Helly, J. C. 2006, *MNRAS*, 368, 1381

- Lippai, A., Frei, Z., & Haiman, Z. 2008 preprint, arXiv:0801:0739
- Loeb, A. 2007, *Phys. Rev. Lett.*, 99, 041103
- Macfadyen, A. I., & Milosavljevic, M. 2008, *ApJ*, 672, 83
- Merritt, D., Milosavljević, M., Favata, M., Hughes, S. A., & Holz, D. E. 2004, *ApJ*, 607, L9
- Milosavljevic, M. & Phinney, E. S. 2008, *ApJ*, 622, L93
- Osterbrock, D. E., & Ferland 2006, 'Astrophysics of Gaseous Nebulae and Active Galactic Nuclei,' 2nd ed., University Science Books
- Salviander, S., Shields, G. A., Gebhardt, K., & Bonning, E. W. 2007, *ApJ*, 662, 131
- Schneider, D. P., et al. 2002, *AJ*, 134, 102
- Schnittman, J. D., & Buonanno, A. 2007, *ApJ*, 662, L63
- Sesana, A., Haardt, F., Madau, P., & Volonteri, M. 2004, *MNRAS*, 347, 1711
- Sesana, A., Volonteri, M. & Haardt, F. 2007, *MNRAS*, 377, 1711
- Shakura, N. I. & Sunyaev, R. A. 1973, *A&A*, 24, 337
- Shields, G. A., Bonning, E. W., & Salviander, S. 2007, to appear in "Black Holes. Poster Papers from the Space Telescope Science Institute Symposium, April 2007, " Mario Livio and Anton Koekemoer, eds., STScI, arXiv:0707:3625.
- Tichy, W. & Marronetti, P. 2007, *Phys. Rev. D*, 76, 061502
- Tremaine, S., et al. 2002, *ApJ*, 574, 740
- Vanden Berk, D., et al. 2001 *AJ*, 122, 549
- Volonteri, M. 2007, *ApJ*, 663, L5

TABLE 1
LINE INTENSITIES OF SHOCK PRECURSOR

Ion	$\lambda(\text{\AA})$	T7.0	T6.3
H β	4861	1.000	1.000
H α	6563	5.0	6.5
Ly α	1215	28.7	88.5
He I	5876	0.10	0.24
He II	304	17.1	19.9
He II	1640	2.7	5.4
He II	4686	0.31	0.68
C II	2326	1.83	0.69
C III	1909	5.1	14.9
C III	977	2.8	2.9
C IV	1549	25.3	55.3
N IV	1486	1.58	5.1
N V	1240	3.52	1.65
O III	1665	2.0	4.7
O IV	1402	2.1	4.8
O V	1218	8.6	1.6
O V	630	5.1	0.03
O VI	1035	48.0	0.44
Mg II	2798	5.2	5.9
Si III	1397	1.6	3.6
$\log N_{\text{H}}$		9.0	8.0
$\log F_{\text{inc}}$		8.77	6.70
$\log F(\text{H}\beta)$		6.34	4.21
EW(H β)		780 \AA	660 \AA
EW(C IV)		6100 \AA	11,500 \AA

NOTE. — Emission-line intensities relative to H β of CLOUDY models for shock precursor zone photoionized by coronal emission spectrum at $10^{7.0}$ or $10^{6.3}$ K(see text). Incident and H β flux in $\text{erg cm}^{-2} \text{ s}^{-1}$. Equivalent widths relative to nebular continuum only.

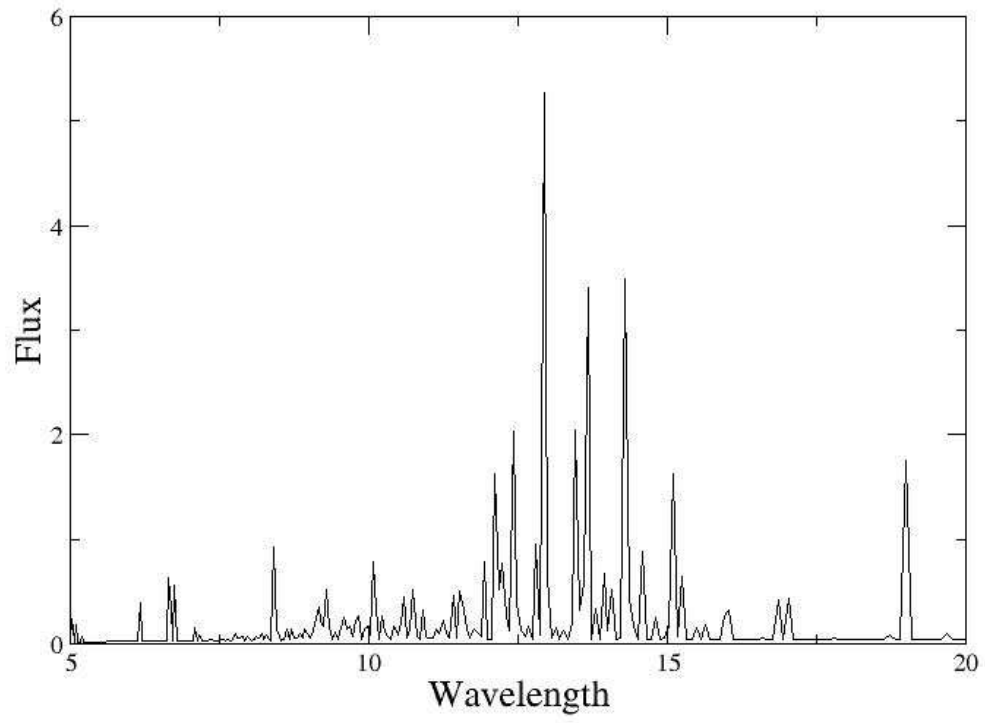


FIG. 1.— Initial configuration ($t = 0$) of simulated accretion disk before recoil of the central black hole (see text). Inner and outer radii are at 10 and 50 in the dimensionless units of the model. Disk rotates counterclockwise seen from above.

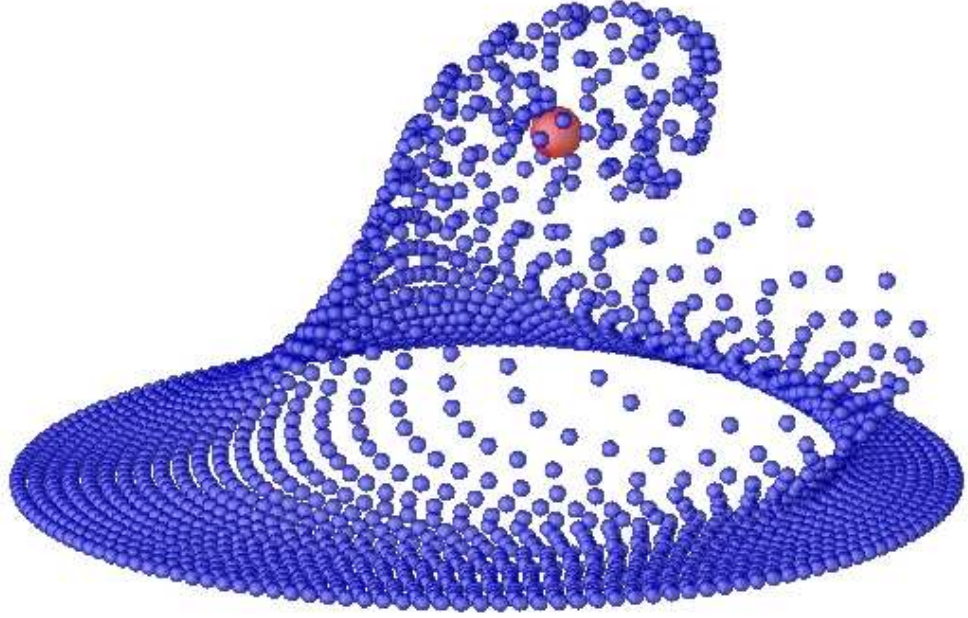


FIG. 2.— Test particle simulation of accretion disk at time $t = 1$ after recoil of the central black hole (see text). In the dimensionless units of the model, the recoil has $v_{\text{kick}} = 65$ and is inclined 45 degrees to the initial disk axis. This corresponds to 65% of the innermost orbital velocity. The pre-kick Keplerian orbital period is $P_b = 2.28$ at the radius $R_b = 23.6$ where $v_{\text{Kep}} = v_{\text{kick}}$. The orbital period at the inner and outer boundaries of the initial disk are $P = 0.63$ and 7.0, respectively.

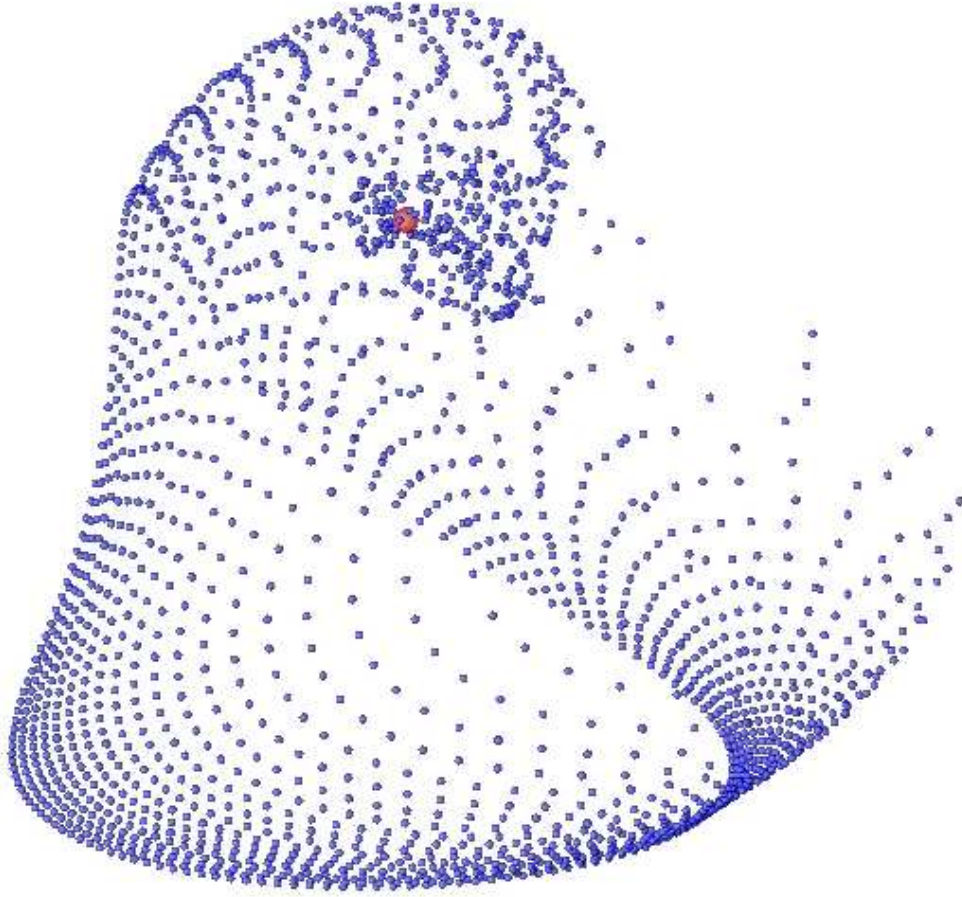


FIG. 3.— Simulated accretion disk at time $t = 2.5 = 1.1P_b$ after recoil of central black hole (see text).

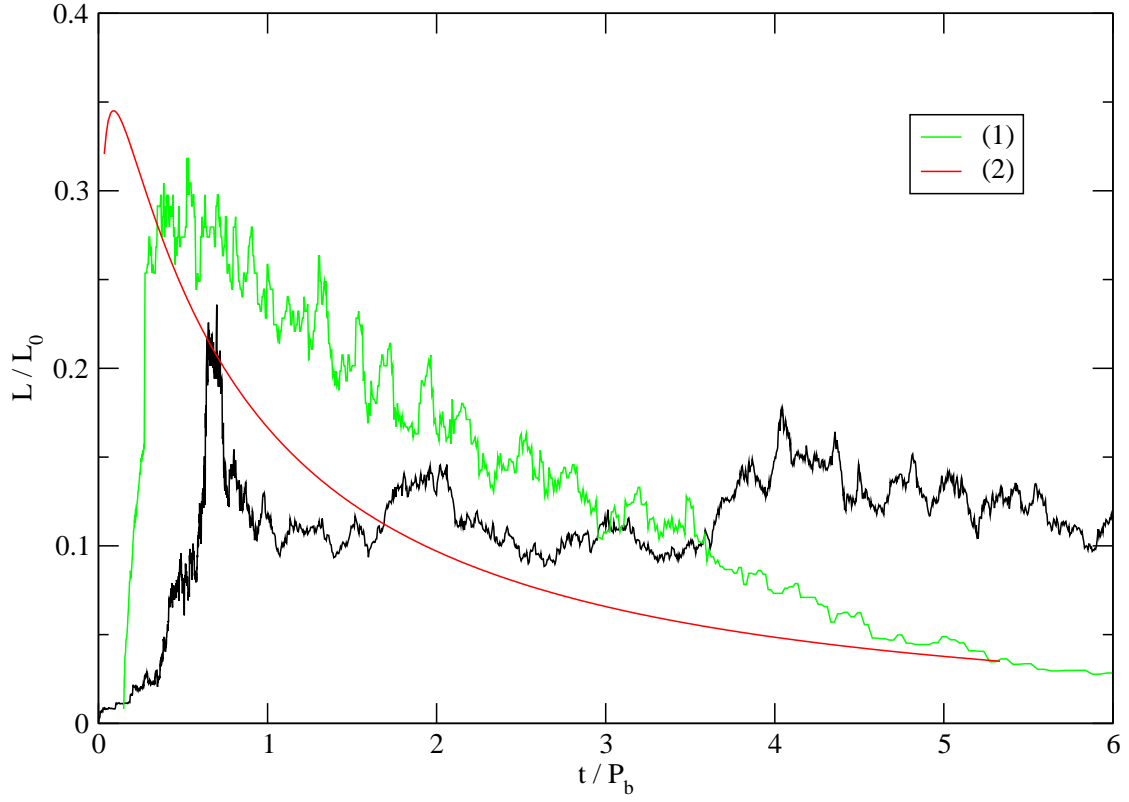


FIG. 4.— Predicted light curves for recoil flare (see text). Black curve with sustained luminosity is power per unit time for particle collisions in numerical simulation; power at later times is overestimated because of repeat collisions. Green curve with declining power is based on post-kick orbital period P of each bound particle, assuming that an energy $(1/2)m_p v_{\text{kick}}^2$ is dissipated at $t = P$. Smooth red curve is analytic solution for axial kick. Each curve is normalized to P_b for the time axis and $L_0 = (1/2)M_b v_{\text{kick}}^2 P_b$ for the luminosity axis. For reference, $P_b = 10^{3.4}$ yr and $L_0 = 10^{45.7}$ erg s $^{-1}$ for $M_{\text{BH}} = 10^8 M_\odot$, $\dot{M} = 10^{-0.5} M_\odot \text{ yr}^{-1}$ and $v_{\text{kick}} = 1000 \text{ km s}^{-1}$ (Equations 4 and 5).

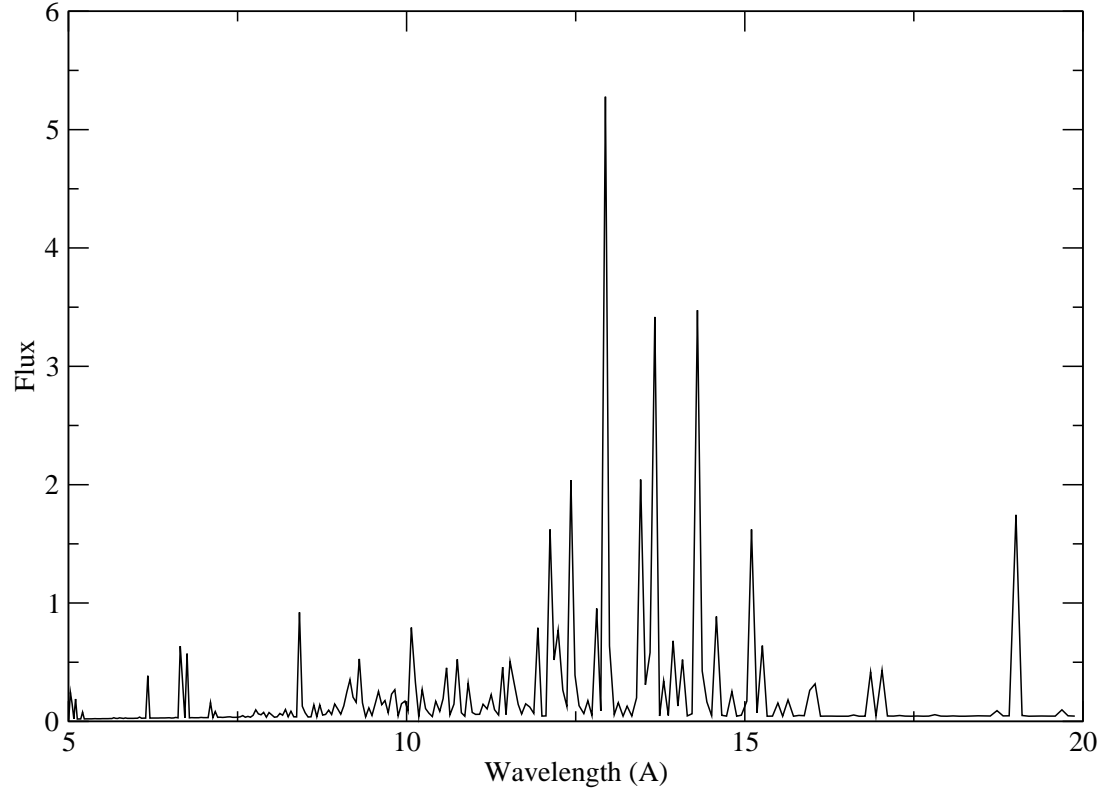


FIG. 5.— Spectrum of optically thin gas in coronal equilibrium at $T = 10^7$ K in wavelength range 5 to 20 Å (see text). Note strong emission lines of Fe xx and neighboring ions. Abscissa is wavelength in Å in bins 1500 km s^{-1} wide; ordinate is λF_λ in arbitrary units. The intrinsic line width for the plot is set at 1000 km s^{-1} .

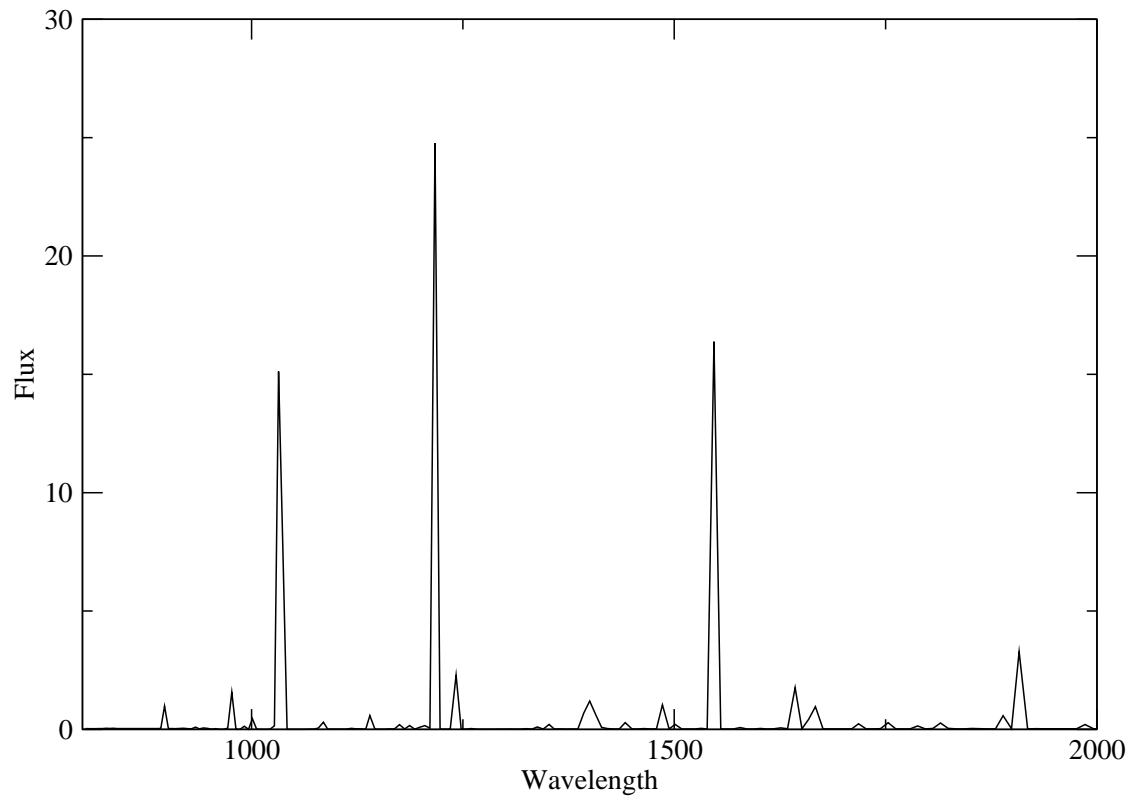


FIG. 6.— Spectrum of photoionized precursor for $T_{\text{shock}} = 10^7$ K in wavelength range 800 to 2000 Å (see text). Note strong emission lines of O VI, Ly α , and C IV. Flux is λF_{λ} in arbitrary units.

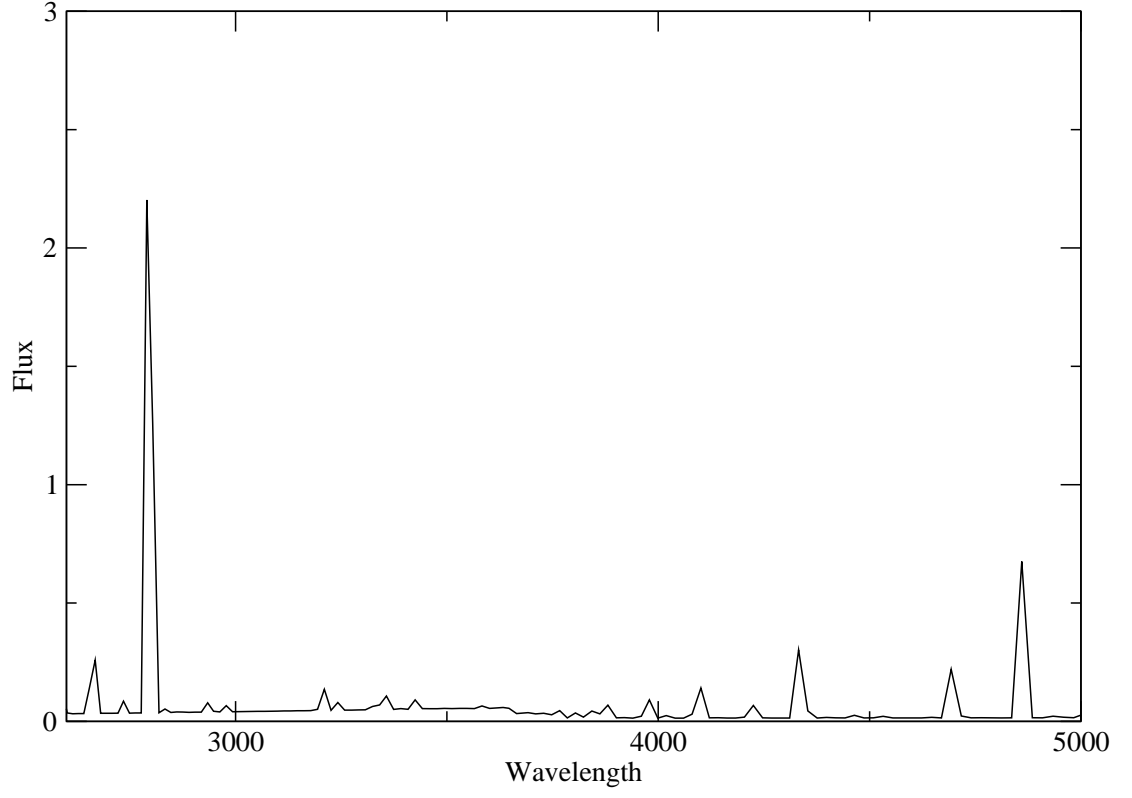


FIG. 7.— Spectrum of photoionized shock precursor for $T_{\text{shock}} = 10^7$ K in wavelength range 2600 to 5000 Å (see text). Flux is λF_{λ} in arbitrary units. Note lines of $\text{H}\beta$, $\text{He II } \lambda 4686$, and Mg II , and Balmer continuum in emission.